Published Online First: August, 2024
https://doi.org/10.21123/bsj.2024.9984
P-ISSN: 2078-8665 - E-ISSN: 2411-7986
Baghdad Science Journal

Preparation and characterization of $NiONP_S$ sensor Prepared by Different Q-switched Nd: YAG Laser parameter: energy pulse and wavelength

Noha. H. Harb

Department of Physics, College of Science for Women, University of Baghdad, Baghdad, Iraq.

Received 18/10/2023, Revised 12/03/2024, Accepted 14/03/2024, Published Online First 20/08/2024

Abstract

In this research, a thin film of nickel oxide was produced by a Q-switched Nd:YAG fundamental laser and third harmonic generation on the porous silicon substrate at different pulse energies. To explore how laser pulse energy and wavelength affect Nickel Oxide thin film characteristics and are used for gas sensor applications. In this investigation, an Nd: YAG laser beam with a wavelength of 1064 and 355nm, 400 pulses, and a repetition rate of 3 Hz was utilized to deposit NiO on porous silicon substrates. The crystal structure of the deposited films was investigated using X-ray diffraction (XRD). The UV-visible spectrum is used to determine the absorption coefficient and optical energy gap, and well as research sensory characteristics. These NiO NPs have a polycrystalline structure and the preferred orientation of <200> for NiO and <100> for PS, according to structural testing. The increase in laser pulse energy correlates favorably with grain size. The optical tests reveal a reduction in wavelength with a rise in the optical energy gap, which is a sign that quantum confinement has formed as an effect of the production of NiO NPs. The impact of temperature variations on the sensitivity, recovery time, and response time of a NO2 gas sensor built from prepared samples was investigated. The maximum sensitivity for NO2 gas at a temperature of 25°C was 134% 190 ppm at 1064 nm and 70% 32 ppm at 355 nm for NiO NPs.

Keywords: Gas sensor, Pulse Laser Deposition, Nickel Oxide, NO_2 gas, Third Harmonic Generation.

Introduction

Gas sensors are key components for detecting dangerous or harmful gases, as well as controlling gaseous pollutants in the environment. The sensors involved must have high sensitivity, low cost and fast detection speeds. The size, range, and detection capabilities of gas sensors vary greatly. Compared to the other types of sensors, gas sensors need to be calibrated more often since they are always in contact with air and other gases. Gas sensors are instruments that convert the concentration of a gas into a meaningful electrical signal[1-4]. The Environmental Protection Agency listed nitrogen oxides as one of the most frequent air contaminants. NO_2 is a key contributor to atmospheric processes that harm the ozone layer, as well as a major source of smog and respiratory difficulties. Constant exposure to such a gas may affect on children's breathing. NO_2 gas is a carcinogenic component of exhaust and cooling systems. Furthermore, the NO_2 gas reacts to generate nitric acid, resulting in acid rain. Developing a selective NO_2 sensor is therefore crucial to tracking the environment for this harmful chemical[5, 6]. Nickel oxide (NiO) could be a promising material in many different kinds of applications, including solar cells, catalysts, detectors, gas sensors, optoelectronic devices, photoconductors, and thermal absorber[7-10].

Published Online First: August, 2024
https://doi.org/10.21123/bsj.2024.9984
P-ISSN: 2078-8665 - E-ISSN: 2411-7986
Baghdad Science Journal

The deposition of nickel oxide has been achieved using manufacturing techniques such as sputtering [11] atomic layer deposition [12], sol-gel[13], spray pyrolysis [14], and pulsed laser deposition (PLD) [15]. A high-power pulsed laser beam is used in the thin-film to vaporize the composition target of choice. PLD has grown in popularity in tandem with advances in laser technology [16]. This technique has advantages and downsides. Benefits include the capacity to employ any kind of ambient gas during deposition, energetic plume, relative safety, convenience, and stoichiometric film deposition[17]. The deposit of micron and sub-micron size particles, as well as the plume's restricted angular dispersion, are the two most significant drawbacks of this method. These limitations are most noticeable when smooth films or large, homogeneous covering regions are needed[18]. High-quality superconducting films have been produced using PLD, magneto-resistant materials, semiconductors, ferroelectrics, and many other materials [19-21]. According to a review of the literature, nickel oxide has various benefits over other p-type MOS and can be a potential sensing material for creating novel chemiresistors [7]. NiO based gas sensors have been utilized to sense several gases, including methanol, xylene, acetone, and hydrogen. Instances of these sensors include NiO/In2O3 [22], Cr doped NiO [23], and NiO-based thin films with Pt surface modifications [24]. Nevertheless, the investigation of NiO structures for NO2 gas sensing received some interest. In this paper, we use the PLD to create high-quality polycrystalline NiO thin films on a porous silicon substrate and investigate laser energies and wavelength effects on the structural, optical and sensing characteristics. The purpose of this research is to offer a promising material for monitoring NO_2 gas in ambient conditions. Nitrogen oxide sensors are one of the most common air pollutants and damage the ozone layer.

Materials and Methods

Silicon wafers of the n-type with a resistivity of 0.1-100 Ohm.cm were washed in HF/ethanol at a 2:1 ratio before being air dried. PS is a nanostructured material created by photo electrochemical etching using a Halogen lamp of 200W Fig. 1. Silicon n-type was used to conduct electrons in a 16 % concentration hydrofluoric acid solution in a Teflon cell using a 20 mA/cm^2.The PLD setup, seen Fig. 2; it is utilized to create NiO high purity 99.999 % on PS substrate. A laser with wavelengths of 1064 nm and 355 nm was used. Ablation conditions include 400 pulses, 3 Hz repetition rate, and 580mJ, 780mJ, and 980mJ laser energy. The crystalline structure was examined utilizing the XRD technique employing a power diffraction system with a Cu-K X-ray tube to calculate the crystallographic size of the NiO Nano partials used Debye Scherrer Eq. 1 [25].

$$D = \frac{0.94\lambda}{\beta \cos\theta} \quad \ldots 1$$

Where (β) is the peak width of the diffraction peak profile at half maximum and (θ) the degree of the diffraction peak. The optical properties of Nickel Oxide thin film were prepared on a glass substrate 3 x 2 cm^2 included absorption, absorption coefficient, and the energy gap measured using a UV-Vis spectrophotometer SP-3000 in the region (200-1100) nm. Applying the following Eq. 2, the absorption coefficient was calculated[25]:

$$\alpha = 2.303 \frac{A}{T} \quad \ldots 2$$

When (A) is the absorption while (T) is the sample thickness. Tauc Eq. 3 has been used to calculate the optical energy gap for NiO films[26, 27].

$$\alpha h\nu = B(h\nu - Eg)^r \quad \ldots 3$$

Where (B) the constant involves the properties of the bands and (υ) frequency of incident photon while(r) is a constant depending on the nature of transition.

The resistance of the specimen was tested in the air, as well as in NO_2 gas, by varying the temperature of the samples between 25-150 degrees Celsius with a bias voltage of 3V applied to electrodes of all specimens. Al electrodes that are 300 nm thick and 0.5 mm apart are embedded in an aluminum foil sheet to form the mask.

The sensitivity could be determined using the Eq. 4 [28].

Published Online First: August, 2024
https://doi.org/10.21123/bsj.2024.9984
P-ISSN: 2078-8665 - E-ISSN: 2411-7986
Baghdad Science Journal

$$S = \frac{R_{on} - R_{off}}{R_{on}} * 100\% \quad \ldots\ldots\ldots\ldots\ldots\ldots\ldots 4$$

Where (R_{on}) resistance before exposure to NO_2 gas while (R_{off}) resistance after exposure to NO_2 gas, the response time and recovery time could be determined using the Eq. 5 and Eq. 6 [28].

$$Response\ time = \left|t_{gas(on)} - t_{gas(off)}\right| * 0.9 \ldots\ldots\ldots\ldots\ldots\ldots\ldots 5$$

$$Recover\ time = \left|t_{gas(off)} - t_{gas(recover)}\right| * 0.9 \ldots\ldots\ldots\ldots\ldots\ldots 6$$

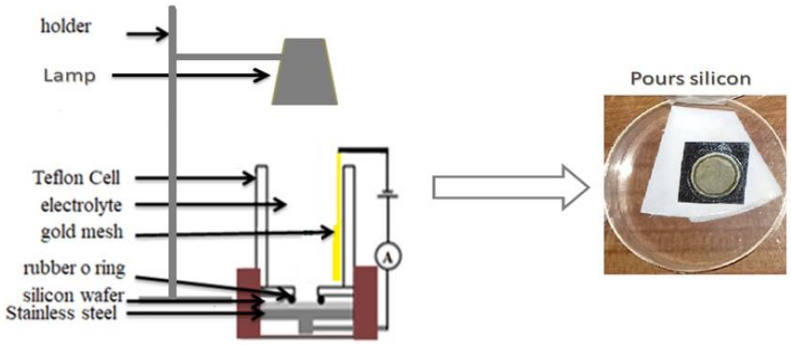

Figure 1. Setup for the experiment of Photo electrochemical Etching system

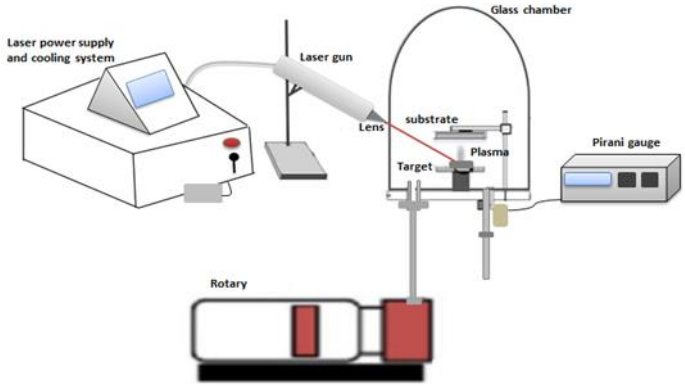

Figure 2. Setup for the experiment of PLD system

Results and discussion

Crystalline characterization of NiONPs

The XRD diffraction peaks of NiO nanoparticle size produced on a Ps substrate, using a pulse laser deposition technique at laser wavelengths 1064 and 355nm, and laser pulse energies 580,780, and 980 mJ, are illustrated in Fig. 3 and Fig. 4. Cub NiO structure can easily index all of the reflection peaks of NiO NPs (JCPDS card No. 96-432-0488), <100> peak connected to the PS substrate. The prominent peak in the XRD diffraction pattern was detected at 43°, this was consistent with the favored orientation in the <200> plane at all wavelengths. Moreover, three reflection peaks were found at 2Θ values of 37 °, 43 ° and 62 °, corresponding to <111>, <200> and <220> Cub NiO reflections, respectively. At wavelengths of 1064 nm for laser pulse energy 980 mJ, Peaks at <111>, <200> and <220> Cub show increasing crystallinity as they get sharper. When high laser energy is added to the atom energy, it results in greater mobility. Finally, the structure recrystallizes and becomes more organized as a result of this. Calculate the crystallographic size of the NiO NPs used Debye Scherrer Eq. 1. The effect of different laser energy on thin film deposition is shown in Table 1 and Table 2. The grain size of the nickel oxide films deposited on the N-type pours silicon substrate wavelength of 1064nm is limited to a range between 13-26 nm while 13-25 nm in wave

Published Online First: August, 2024
https://doi.org/10.21123/bsj.2024.9984
P-ISSN: 2078-8665 - E-ISSN: 2411-7986
Baghdad Science Journal

length 355nm. Increasing the energy of lasers with increasing crystallite size, the FWHM to drop, although it is somewhat displaced to a smaller refraction angle.

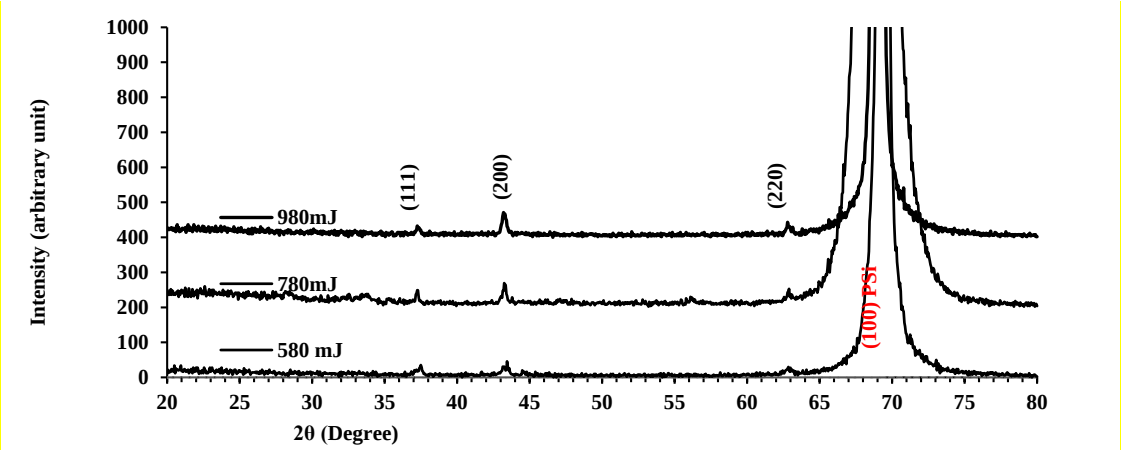

Figure 3. The X-ray diffraction peaks of NiO grown on Ps substrate with different laser pulse energies and an Nd: YAG laser 1064 nm.

Table 1. The X-ray diffraction data of NiO grown on Ps substrate with different laser pulse energies and an Nd: YAG laser 1064 nm.

Laser energy/1064nm	2θ (Deg.)	FWHM (Deg.)	d_{hkl} Exp.(Å)	C.S (nm)	hkl
580mJ	37.4641	0.6160	2.39862	13.6	(111)
	43.3470	0.5544	2.08574	15.4	(200)
	62.8439	0.5853	1.47755	15.9	(220)
780mJ	37.2793	0.3464	2.41009	24.2	(111)
	43.2854	0.3380	2.08857	25.3	(200)
	62.9363	0.3696	1.4756	25.2	(220)
980mJ	37.2485	0.3388	2.41201	24.7	(111)
	43.2546	0.3188	2.08998	26.8	(200)
	62.7823	0.3496	1.47885	26.6	(220)

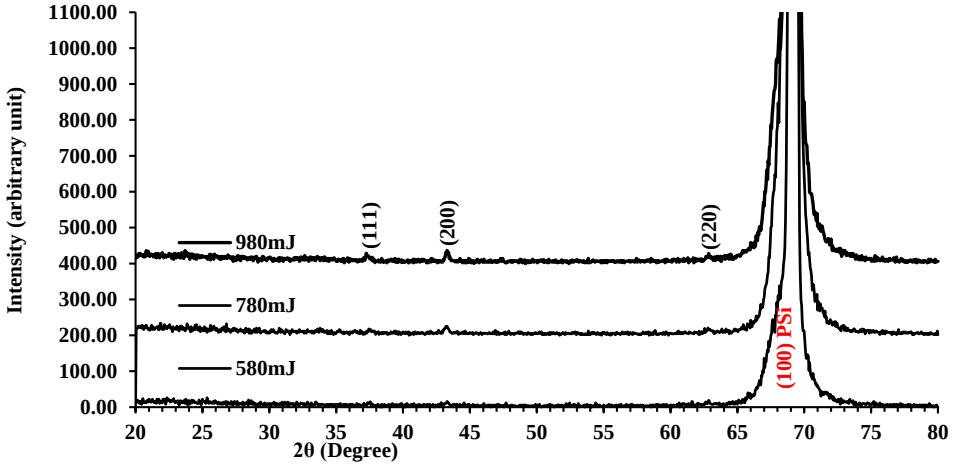

Figure 4. The X-ray diffraction peaks of NiO grown on Ps substrate with different laser pulse energies and an Nd: YAG laser 355 nm.

Published Online First: August, 2024
https://doi.org/10.21123/bsj.2024.9984
P-ISSN: 2078-8665 - E-ISSN: 2411-7986
Baghdad Science Journal

Table 2. The X-ray diffraction data of NiO grown on Ps substrate with different laser pulse energies and an Nd: YAG laser 355 nm.

Laser energy/355nm	2θ (Deg.)	FWHM (Deg.)	d_{hkl} Exp.(Å)	C.S (nm)	hkl
580mJ	43.3028	0.4403	2.08777	19.4	(200)
	37.4312	0.4110	2.40065	20.4	(111)
780mJ	43.2661	0.4137	2.08945	20.7	(200)
	62.8257	0.5505	1.47793	16.9	(220)
980mJ	37.3945	0.3500	2.40293	24.0	(111)
	43.3028	0.3302	2.08777	25.9	(200)
	62.8257	0.3700	1.47793	25.2	(220)

Optical characterization of NiONPs

Fig. 5 (a and b) It was noticed that when using the Nd: YAG laser wavelength of 1064 nm and energies 580,780 ,and 980 mJ the maximum absorption range was 292-318 nm, whereas when using the Nd: YAG laser wavelength of 355 nm and energies 580,780 ,and 980 mJ the maximum absorption was at 298-322 nm . In the two figures demonstrated, it can be seen that the shorter wavelength led to a higher absorbance with a larger value, indicating the presence of a lot of produced NPs in the thin film. As the energy is increased, the absorption peak rises. In terms of the laser wavelength effect, a drop in wavelength results in an increase in absorbance with increasing laser energy.

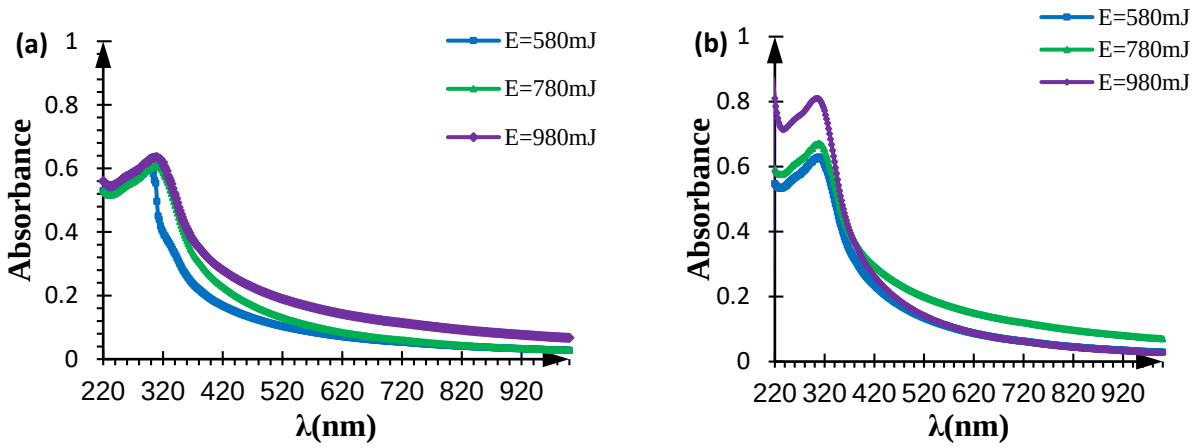

Figure 5. The relationship between absorption fluctuation and wavelength for NiO grown on glass substrate for Nd: YAG laser a. 1064nm and b.355nm.

The kind and size of the optical band gap may be determined via the fundamental absorption edge of that thin film, which relates to electron excitation in the valance band to the conduction band. A region with high absorption in the film's fundamental absorption edge served as the basis for calculating the absorption coefficient. In Fig. 6(a and b), we demonstrate how the absorption coefficient (α) varies for NiO thin film when the laser wavelength is utilized at 1064 nm and 355 nm, respectively. Applying the following Eq. 2, the absorption coefficient was calculated. This figure illustrates how the researched NiO thin films absorb more light as laser pulse energy is increased. The absorption coefficient for the NiO thin films under investigation rises with increasing photon energy, as can be observed from the figures. An absorption coefficient with a value of $>10^4$ cm^{-1} increases the likelihood of a direct transition occurring. While the absorption coefficient rises as the wavelength does. This is related to the formation phase, the growth of layer density and grain size, and the effect of light scattering on the high surface roughness.

Published Online First: August, 2024
https://doi.org/10.21123/bsj.2024.9984
P-ISSN: 2078-8665 - E-ISSN: 2411-7986
Baghdad Science Journal

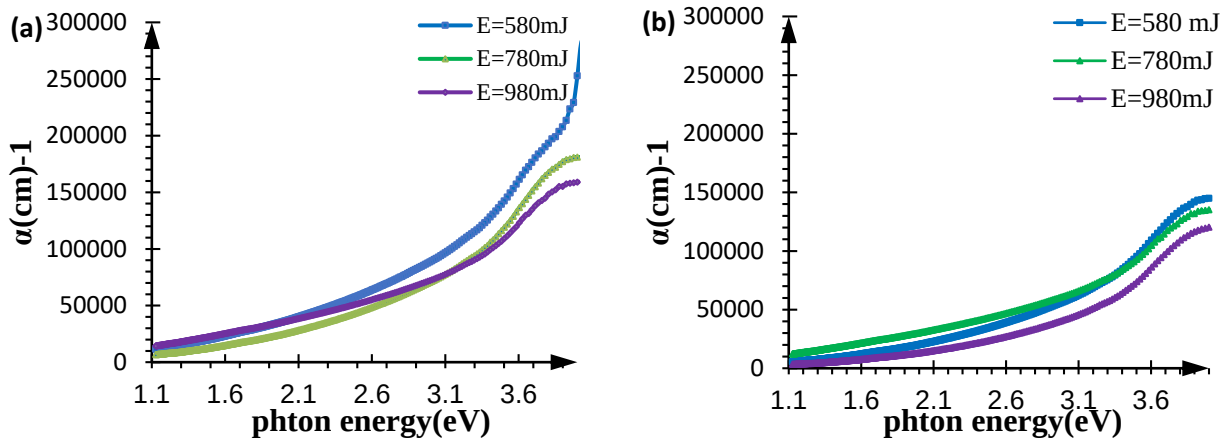

Figure 6. The relationship between the absorption coefficient fluctuation and photon energy for NiO grown on glass substrate at Nd: YAG laser for a. 1064nm and b.355nm.

The crystal structure of the thin film, as well as the distribution and arrangement of atoms inside the crystal lattice, all affect the Eg values. Tauc Eq. 3 has been used to calculate the optical energy gap values Eg for NiO thin film. In Fig. 7(a and b), we find that energy gap at 1064 nm increased by increasing pulses energy laser its range 3.43eV to 3.52 eV where the highest value was when the energy pulses laser (980 mJ), while its values, in general, increased by increasing energy pulses laser at 355 nm and its range 3.4 eV to 3.5 eV this is due to the regularity of the prepared particles morphology at this wavelength, according to XRD analyzes.

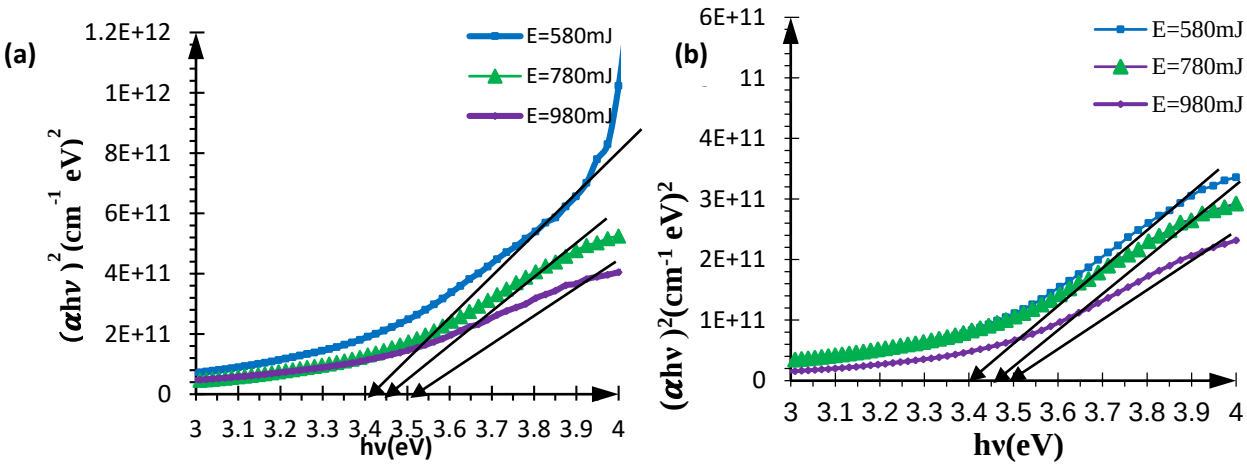

Figure 7. The relationship between $(\alpha h\upsilon)^2$ versus $h\upsilon$ for NiO thin films prepared by PLD technique for a. 1064nm and b.355nm.

Characterizations Gas Sensor of NiO NPs

Resistance varies when the sensor is subjected to a given concentration of gas, as well as the elements that impact sensitivity such as the sensor operating temperature, doping, and crystal size. The appropriate parameters of the detector should be studied to increase the sensitivity's efficiency.

Fig. 8 (a, b) demonstrates the variation of sensitivity with operation temperature in the domain from 25°C to 150°C, of the NiO NPs films prepared with different laser energies 580, 780, and 980 mJ as gas sensors for NO_2 gas at wavelengths of 1064 nm and 355 nm, respectively. The sensitivity could be determined using the Eq. 4.

The large sensitivity of deposition at different laser pulse energy increased at temperature 25 °C, then decreased at 100 and after increased at 150°C. Because the gas absorption and dissociation rate of

Published Online First: August, 2024
https://doi.org/10.21123/bsj.2024.9984
P-ISSN: 2078-8665 - E-ISSN: 2411-7986
Baghdad Science Journal

the sensor's surface rises, the sensor's sensitivity falls. Operating temperature sets a limit on sensing performance, which in turn establishes critical sensing characteristics including selectivity, responsiveness, and recovery durations[29]. The temperature of 25°C was found to have a higher sensitivity, which was taken into account. The highest sensitivity 134% 190ppm at 580 mJ for NO2 gas is utilized as the probing gas at wavelength 1064nm and the highest sensitivity is 70% 32ppm at 780 mJ at wavelength 355nm. The effect of different laser energy and wavelengths on Gas Sensor characters is shown in Table 3 and Table 4

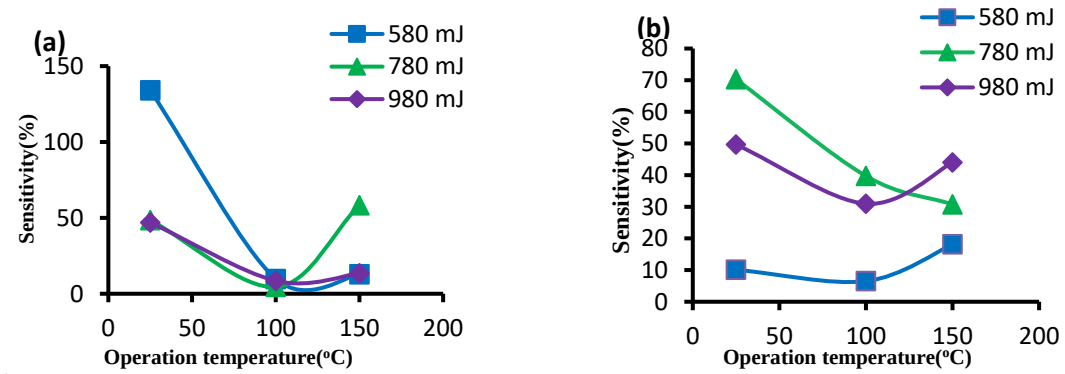

Figure 8. The fluctuation of sensitivity at varied operation temperatures for NiO NPs/PS samples created at different laser pulse energy for a. 1064nm and b.355nm.

Fig. 9 and Fig. 10 illustrate the reaction time and recovery time of the NiO NPs films prepared with different laser energies 580, 780, and 980 mJ at wavelengths of 1064 nm and 355 nm. The sample response time is the gas reaction time, and the sample recovery time is the amount of time it takes for the sample to get back to how it was before pumping the gas. Eq. 5 and Eq. 6 have been used to calculate that the highest reaction time 32.4sec was achieved at 25°C, while the shortest recovery time 50.4sec was achieved at 100°C laser wavlength1064nm. The highest reaction time 34.2sec was achieved at 25°C, while the shortest recovery time 37.8sec was achieved at 150°C laser wavlength355nm. Due to grain development and porosity effects, the optimum reaction time was obtained at 25°C at all laser wavelength. The adsorption and desorption are temperature dependent thermal processes, therefore the NiO NPs sensor recovery time is quickest at low temperatures and slows as the temperature rises.

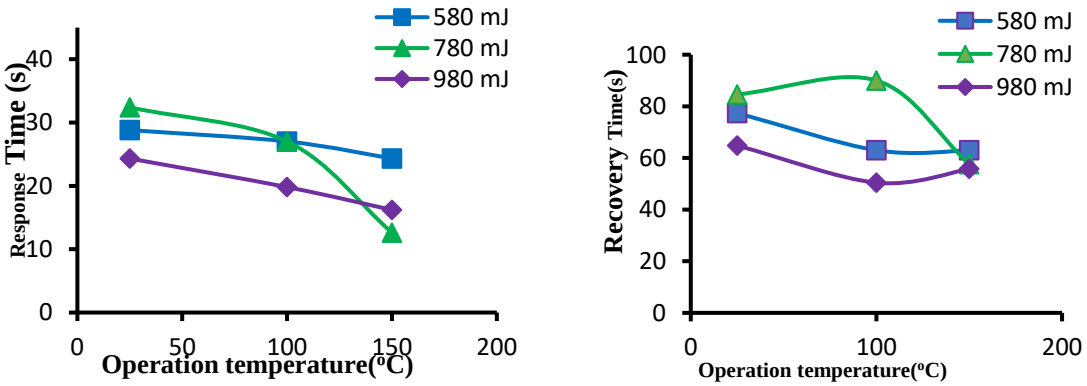

Figure 9. The fluctuation of response time and recovery time of the NiO NPs at varied operation temperatures and laser pulse energy at 1064nm

Published Online First: August, 2024
https://doi.org/10.21123/bsj.2024.9984
P-ISSN: 2078-8665 - E-ISSN: 2411-7986
Baghdad Science Journal

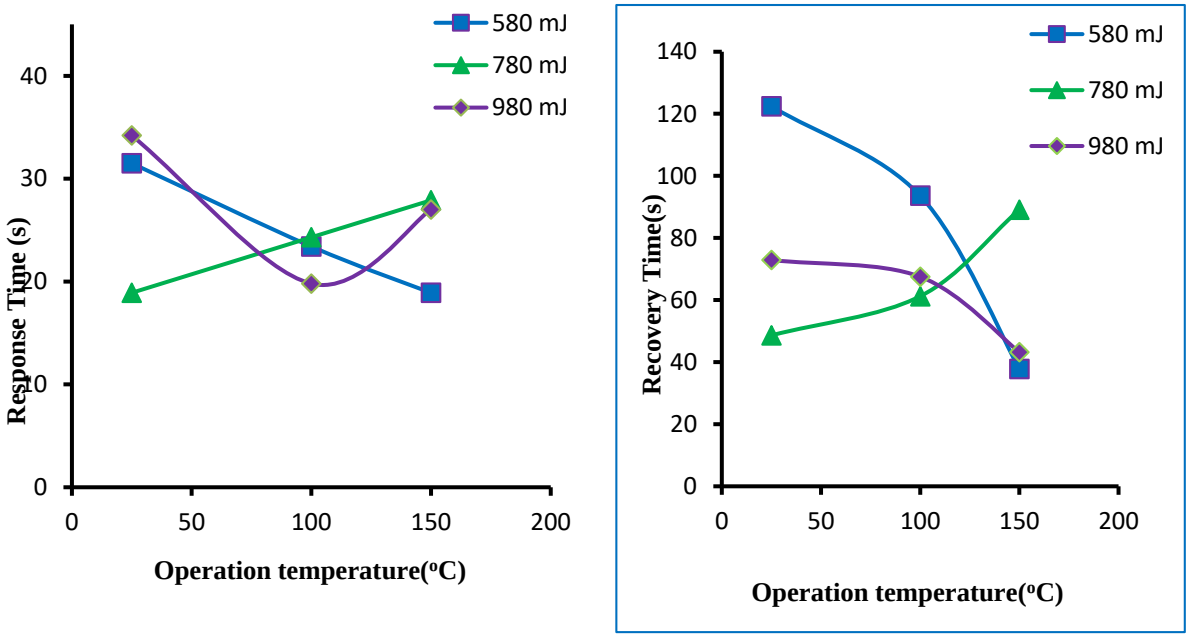

Figure 10. The fluctuation of response time and recovery time of the NiO NPs at varied operation temperatures and laser pulse energy at 355nm

Table 3. Values of characterizations Gas Sensor of NiO NPs before and after exposure NO_2 gas different laser pulse energy and an Nd: YAG laser 1064 nm.

Laser energy	T°C	sensitivity %	response time(sec)	recover time (sec)
580 mJ	25	134.0715503	28.8	77.4
	100	9.798270893	27	63
	150	12.91262136	24.3	63
780 mJ	25	48.5334608	32.4	84.6
	100	4.569606801	27	90
	150	58.4	12.6	57.6
980 mJ	25	47.00315457	24.3	64.8
	100	8.535489668	19.8	50.4
	150	13.58629131	16.2	55.8

Table 4. Values of characterizations Gas Sensor of NiONPs before and after exposure NO_2 gas different laser pulse energy and an Nd: YAG laser 355 nm.

Laser energy	T°C	sensitivity %	response time(sec)	recover time (sec)
580 mJ	25	10.1010101	31.5	122.4
	100	6.502242152	23.4	93.6
	150	18.16275168	18.9	37.8
780 mJ	25	70.27027027	18.9	48.6
`	100	39.72550515	24.3	61.2
	150	30.72550515	27.9	89.1
980 mJ	25	49.63636364	34.2	72.9
	100	30.95412844	19.8	67.5
	150	44.00781454	27	43.2

Published Online First: August, 2024
https://doi.org/10.21123/bsj.2024.9984
P-ISSN: 2078-8665 - E-ISSN: 2411-7986
Baghdad Science Journal

Conclusion

The study confirmed that the successful fabrication of NiO nanoparticles by laser pulsed deposition with different parameters (energy and wavelength) at ambient temperature had potential as functional materials for the nitrogen oxide sensor, which is one of the most common air pollutants. Our results demonstrate that the film's thickness, form, and sensing properties can be controlled by modifying the laser's settings. The energy of lasers impacts the crystallinity of the peak. Increasing the laser fluence leads to improved crystallinity quality, as evidenced by the narrowing of the XRD peaks. The optical tests reveal a direct transition occurring, and the energy gap increased by increasing pulses of energy laser is due to the regularity of the prepared particle morphology. The NiO NP sensor recovery time accelerates at low temperatures and slows as the temperature rises. Because adsorption and desorption are temperature-dependent thermal processes, as the operating temperature rises, electron transport from the conductor band to the surface Fermi level accelerates, speeding up the adsorption reaction and shortening the recovery time.

Author's Declaration

- Conflicts of Interest: None.
- I hereby confirm that all the Figures and Tables in the manuscript are mine. Furthermore, any Figures and images, that are not mine, have been included with the necessary permission for re-publication, which is attached to the manuscript.
- No animal studies are present in the manuscript.
- No human studies are present in the manuscript.
- Ethical Clearance: The project was approved by the local ethical committee at University of Baghdad.

References

1. Hunter G W, Akbar Sh , Bhansali Sh, Daniele M, Erb P D, Johnson K et al. Editors' Choice—Critical Review—A Critical Review of Solid State Gas Sensors. ECS Sens Plus. 2020; 167(3): 037570. https://doi.org/10.1149/1945-7111/ab729c
2. Peng Li, Lin Lü. Evaluating the Real-World NOx Emission from a China VI Heavy-Duty Diesel Vehicle. Appl Sci. 2021; 11(3): 1335. https://doi.org/10.3390/app11031335
3. Harb N H , Falah MuAtlak F A-H.Gas sensing characteristics of WO3NPs sensors fabricated by pulsed laser deposition on PS n-type. J Opt 2023; 52 (1): 323-331. https://doi.10.1007/s12596-022-00877-1
4. Ch, Luo Y, Debliquy M. Room temperature conductive type metal oxide semiconductor gas sensors for NO2 detection. Sens Actuators A Phys. 2019; 289(15): 118-133. https://doi.org/10.1016/j.sna.2019.02.027
5. Huang Z, Wei Z, Tang M, Yu Sh, Jiao H. Chap 3 - Biological treatments of mercury and nitrogen oxides in flue gas: biochemical foundations, technological potentials, and recent advances. Advances in Applied Microbiology. 2021; 116: 133-168. https://doi.org/10.1016/bs.aambs.2021.04.001
6. Licznerski B .Thick-film gas microsensors based on tin dioxide. Bull. Pol Ac: Tech.2004; 52(1): 37-42.
7. Nada K. Abbas,Isam M. Ibrahim,Manal A. Saleh. Characteristics of MEH-PPV/Si and MEH-PPV/PS Heterojunctions as NO2 Gas Sensors. Silicon. 2018; 10(4): 1345–1350. https://doi.org/10.1007/s12633-017-9610-5
8. Chen Y L, Huang Y J, Yeh M H, Fan M S, Lin Ch T, Chang Ch Ch. Nanoflower-like P-doped Nickel Oxide as a Catalytic Counter Electrode for Dye-Sensitized Solar Cells. Nanomaterials 2022; 12(22): 4036. https://doi.org/10.3390/nano12224036
9. Zijun Hu, Chen Da, Yang P, Yang L, Yang L, Qi n L, et al.. Sol-gel-processed yttrium-doped NiO as hole transport layer in inverted perovskite solar cells for enhanced performance. Appl Surf Sci. 2018; 441(31): 258-264. https://doi.org/10.1016/j.apsusc.2018.01.236
10. Akinkuade Sh T, Meyer W E, Nel J M. Effects of thermal treatment on structural, optical and electrical properties of NiO thin films. Physica B. 2019; 575: 411694. https://doi.org/10.1016/j.physb.2019.411694
11. Prajesh R, Goyal V, Nahid M, Saini V, Nahid M. Saini V, et al. .Nickel oxide (NiO) thin film optimization by reactive sputtering for highly sensitive formaldehyde sensing. Sens Actuators B Chem. 2020;

Published Online First: August, 2024
https://doi.org/10.21123/bsj.2024.9984
P-ISSN: 2078-8665 - E-ISSN: 2411-7986
Baghdad Science Journal

318: 128166. https://doi.org/10.1016/j.snb.2020.128166
12. Bonomo M. Synthesis and characterization of NiO nanostructures: a review. J Nanopart Res. 2018; 20(8): 1-26. https://doi.org/10.1007/s11051-018-4327-y
13. Tatyana Ivanova T, Harizanova A, Shipochka M, Vitanov P. Nickel Oxide Films Deposited by Sol-Gel Method: Effect of Annealing Temperature on Structural, Optical, and Electrical Properties. Materials. 2022; 15(5): 1742. https://doi.org/10.3390/ma15051742
14. López-Lugo V H, Hipólito MG, Gómez AR, Alonso-Huitrón JC. Fabrication of Li-Doped NiO Thin Films by Ultrasonic Spray Pyrolysis and Its Application in Light-Emitting Diodes. Nanomaterials (Basel). 2023; 13(1): 197. https://doi.org/10.3390/nano13010197
15. Kumar Yadav S K, Dhar S. Very thin (111) NiO epitaxial films grown on c-sapphire substrates by pulsed laser deposition technique. Semicond Sci Technol. 2021; 36(5):8. https://doi.org/10.1088/1361-6641/abed8e
16. Mazhir S N, Harb N H. Influence of concentration on the structural, optical and electrical properties of TiO2: CuO thin film Fabricate by PLD. J Appl Phys. 7(6): 14-21. https://doi.org/10.9790/4861-07621421
17. Dalya K. Naser , Ahmed K. Abbas, Kadhim A. Aadim, Zeta Potential of Ag, Cu, ZnO, CdO and Sn Nanoparticles Prepared by Pulse Laser Ablation in Liquid Environment. Iraqi J Sci. 2020; 61(10): 2570-2581. https://doi.org/10.24996/ijs.2020.61.10.13
18. Mutlak F A-H, Jamal R K, Ahmed AF. Pulsed Laser Deposition of Tio2 Nanostructures for Verify the Linear and Non-Linear Optical Characteristics. Iraqi J Sci. 2021; 62(2): 517-525. https://doi.org/10.24996/ijs.2021.62.2.18
19. Mahdi1 Sh S, Aadim K A, Khalaf M A. New Spectral Range Generations from Laser-plasma Interaction. Baghdad Sci J. 2021; 18(4): 1328-1337. http://dx.doi.org/10.21123/bsj.2021.18.4.1328
20. Badica P, Togano K, Awaji S and Watanabe K.Growth of superconducting MgB 2 films by pulsed-laser deposition using a Nd–YAG laser. Supercond Sci Technol. 2006; 19(2): 242. https://doi.org/10.1088/0953-2048/19/2/016
21. Oguz Er A, Ren W Elsayed-Ali H E. Low temperature epitaxial growth of Ge quantum dot on Si (100)-(2×1) by femtosecond laser excitation. Appl Phys. 2011; 98(1): 013108. https://doi.org/10.1063/1.3537813
22. Amarnath.M, Gurunathan.K. Highly selective CO2 gas sensor using stabilized NiO-In2O3 nanospheres coated reduced graphene oxide sensing electrodes at room temperature. Sens Actuators B. 2018; 268 : 223–231. https://doi.org/10.1016/j.jallcom.2020.157584
23. Peipei Li, Changyan Cao, Qikai Shen, Bin Bai, Hon gqiang Jin, Jia Yu, et al. Cr-doped NiO nanoparticles as selective and stable gas sensor for ppb-level detection of benzyl mercaptan. Sens Actuators B. 2021; 339: 129886. https://doi.org/10.1016/j.snb.2021.129886
24. Huey-Ing C, Hsiao C, Wei-Cheng Ch, Ching-Hong Ch, Chou T, Liu I, et al. Characteristics of a Pt/NiO thin film-based ammonia gas sensor. Sens Actuators B 2018 ; 256: 962-967. https://doi.org/10.1016/j.snb.2017.10.032
25. Abdul-Ameer H J , AL-.Hilli M F , Khalaf M K. Comparative NO2 Sensing Characteristics of SnO2:WO3 Thin Film Against Bulk and Investigation of Optical Properties of the Thin Film. Baghdad Sci J. 2018; 15(2): 227-233. http://dx.doi.org/10.21123/bsj.2018.15.2.0227
26. Abbas N K, Abdulameer A F, Ali R M, Alwash S M. The Effect of Heat Treatment on Optical Properties of Copper (II) Phthalocyanine Tetrasulfonic Acid Tetrasodium Salt (CuPcTs) Organic Thin Films. Silicon, 2019; 11(2): 843–855. https://doi.org/10.1007/s12633-018-9874-4
27. Harb N H, The structure and optical properties of Ag doped CdO thin film prepared by pulse laser deposition (PLD), Baghdad Sci J. 2018; 15 (3) : 300–303. https://doi.org/10.21123/bsj.2018.15.3.0300
28. Nayef U, Kamel R. Bi2O3 nanoparticles ablated on porous silicon for sensing NO2 gas. Optik. 2020; 208: 164146. https://doi.org/10.1016/j.ijleo.2019.164146
29. Kannan S, Rieth L, Solzbacher F. NO x sensitivity of In $_2$O $_3$ thin film layers with and without promoter layers at high temperatures. Sens Actuators B: Chem. 2010; 149: 8-19. http://dx.doi.org/10.1016/j.snb.2010.06.042

Published Online First: August, 2024
https://doi.org/10.21123/bsj.2024.9984
P-ISSN: 2078-8665 - E-ISSN: 2411-7986
Baghdad Science Journal

تحضير وتوصيف مستشعر جسيمات النيكل النانوية المُحضر بواسطة ليزر النديميوم –ياك بمعلمات ليزرمختلفة: نبضة طاقة الليزر والطول الموجي

نهى حسن حرب

قسم الفيزياء، كلية العلوم للبنات، جامعة بغداد، بغداد، العراق.

الخلاصة

في هذا البحث، تم تحضير طبقة رقيقة من اوكسيد النيكل بتقنية ليزرQ-switched Nd: YAG الاساسي والتوليف التوافقي الثالث على ركائز من السيليكون المسامي بطاقات نبضيه مختلفة. من أجل بيان مدى تأثير طاقة الليزروالطول الموجي على خصائص الأغشية الرقيقة واستخدام مادة أكسيد النيكل في تطبيقات مستشعرات الغاز. استخدام شعاع ليزر Nd: YAG بطول موجي 1064 و355 نانومتر، 400 نبضة ومعدل تكرار 3 هرتز لترسيب NiO على ركائز السيليكون المسامية . التركيب البلوري للأغشية المودعة باستخدام حيود الأشعة السينية (XRD). استخدام الطيف المرئي والأشعة فوق البنفسجية لتحديد معامل الامتصاص وفجوة الطاقة الضوئية، كما تمت دراسة الخصائص التحسسية. تتمتع NiO NPs ببنية متعددة البلورات واتجاه مفضل قدره <200> لـ NiO و<100> لـ PS، وفقًا للاختبارات الهيكلية. ترتبط الزيادة في طاقة نبض الليزر بشكل إيجابي بحجم الحبوب. تكشف الاختبارات البصرية عن انخفاض في الطول الموجي مع ارتفاع في فجوة الطاقة الضوئية، وهذ يبين ان الحبس الكمي قد تشكل كتأثير لإنتاج NiO NPs. تمت دراسة تأثير التغيرات في درجات الحرارة على حساسية وزمن الاسترداد والاستجابة لمستشعر غاز ثاني أكسيد النيتروجين للعينات المحضرة. كانت الحساسية القصوى لغاز NO_2 عند درجة حرارة 25 درجة مئوية هي 134% 190 جزء في المليون عند 1064 نانومتر و70% 32 جزء في المليون عند 355 نانومتر بالنسبة لـ NiO NPs

الكلمات المفتاحية: المتحسس الغازي، الترسيب بالليزر النبضي، اوكسيد النيكل؛ غاز اوكسيد النيتروجين، الجيل التوافقي الثالث.